Supplementary Information (SI) for Chemical Science.
This journal is © The Royal Society of Chemistry 2024

Multipodal Au-C grafting of calix[4]arene molecules on gold nanorods

Electronic Supplementary Information

Auguste Tetenoire,[a] Anna Omelchuk,[a] Volodymyr Malytskyi,[b] Ivan Jabin,[b] Victor Lepeintre,[b,c] Gilles Bruylants,[c] Yun Luo,[d] Arnaud Fihey,[a] Mikaël Kepenekian,*[a] and Corinne Lagrost*[a]

[a] *Univ Rennes, CNRS, ISCR (Institut des Sciences Chimiques de Rennes) - UMR 6226, F-35000 Rennes, France*
[b] *Laboratoire de Chimie Organique, Université libre de Bruxelles (ULB), Avenue F. D. Roosevelt 50, CP160/06, B-1050 Brussels, Belgium*
[c] *Engineering of Molecular NanoSystems, Ecole Polytechnique de Bruxelles, Université libre de Bruxelles (ULB), Avenue F. D. Roosevelt 50, CP165/64, B-1050 Brussels, Belgium*
[d] *Université Paris Cité, CNRS, Laboratoire de Chimie et de Biochimie Pharmacologiques et Toxicologiques, F-75006 Paris, France*

E-mails: mikael.kepenekian@univ-rennes.fr; corinne.lagrost@univ-rennes.fr

Contents

1 Gold nanorods synthesis and functionalization

1.1 Chemicals

Solvents and reagents for the syntheses were at least of reagent grade quality and used without further purification. $HAuCl_4.3\ H_2O$ was purchased from Alfa Aesar, $NaBH_4$, ascorbic acid, CTAB, silver nitrate were purchased from Sigma-Aldrich. Ultrapure water with a resistivity of 18.2 MΩ.cm was used to prepare the aqueous solutions. $X_4N_2^+$ and $X_4(N_2^+)_4$ salts were synthesized as previously published.[1–3]

1.2 Nanorods synthesis

Previously, all flasks and stirring bars were washed with an aqua-regia solution. The gold nanorods were prepared following a previously published procedure by using the seed growth method.[4] The seed solution was prepared by mixing 5 mL of aqueous 0.2 M CTAB and 5 mL of aqueous 5.10^{-4} M $HAuCl_4$ at 30-35°C. After vigorous stirring, 600 μL of ice-cold aqueous 10^{-2} M $NaBH_4$ was added dropwise, then after 2 min we obtained a light brown transparent solution and stirring was stopped. The solution was kept aging at 30°C for 60 minutes before use. In the meantime, the growth solution was prepared as follows. First, 1 mL of aqueous 4.10^{-3} M $AgNO_3$ was added to 50 mL of aqueous 0.2 M CTAB at 30-35°C, after stirring solution was kept undisturbed during 15 minutes. Then, 50 mL of 10^{-3} M $HAuCl_4$ were added under smooth stirring. After slow agitation for 15 minutes, we could observe a dark yellow solution. Further addition of 700 μL of ascorbic acid (78 mM) to the solution leads to a change of color from yellow-brown to white. Agitation was stopped after 30 seconds of a very intense mixture stirring. Finally, 120 μL of the seed solution was added to the growth solution at 30-35°C. After 30 minutes, the color of the solution became deep blue. The stirring was stopped and the AuNRs were kept undisturbed during 2 hours to let them grow along the longitudinal axis. The gold nanorods were purified by three centrifugation steps (5000 rpm during 20 minutes), allowing the elimination of excess of CTAB and/or unreacted products. The gold nanorods were finally redispersed in pure water.

1.3 Functionalization of gold nanorods

10 mL of gold nanorods in aqueous solution (OD = 0.8 - 1) were mixed with 1 mL of an ice-cold 50 mM $NaBH_4$ for 40 min.[5] Then, 1 mL of a solution of $X_4N_2^+$ or $X_4(N_2^+)_4$ salts ($\sim 10^{-3}$ M) in acetonitrile is added to the mixture, and left to incubate overnight ($\sim$18h) at room temperature. The nanorods were purified through a centrifugation step (10 min, 10000 rpm) where the orange supernatant was removed. The functionalized gold nanorods were redispersed in 5 mM NaOH or in pure water. The suspension is stable and stored in the fridge until use.

2 Methods

2.1 High resolution transmission electron microscopy

High resolution transmission electron microscopy (HRTEM) images were recorded using a Jeol 2100 microscope with an acceleration voltage of 200 kV and a Gatan Orius 200-CCD camera. The gold nanorods were diluted in water, and one drop of this dispersion was deposited on a carbon grid. The electronic absorption spectra of the gold nanorods dispersion were recorded with a spectrophotometer Shimadzu UV3600 Plus in quartz cuvettes.

2.2 X-ray photoelectron spectroscopy

XPS measurements were performed onto a deposit of nanorods colloids onto a silicon substrate. The XPS data have been collected with a Kratos Axis Nova spectrometer at Institut des Matériaux de Nantes (France), using the Al Kα X-Ray source (1486.6 eV) and using a spot size of 0.7$\times$0.3 mm^2. Survey spectra (0-1000 eV) were acquired with an analyzer pass energy equal to 160 eV (0.5 eV/step, dwell time 10 s) while the high-resolution spectra used a pass energy of 40 eV (0.1 eV/step, dwell time between 100 and 500 s). Binding energy were referenced to Au4f5/2 peak at 83.9 eV. The core level spectra were further peak-fitted using the CasaXPS software, Ltd Version 2.3.25.6 U2 Tougaard or Shirley background were employed as baseline. The peak areas were normalized by the manufacturer-supplied sensitivity factor (SC_{1s} = 1, S_{Au4f}= 17.12, S_{O1s} = 0.78, S_{Br3p} = 5.03, S_{N1s} = 1.8).

2.3 Raman spectroscopy

Raman spectra were acquired with a ThermoFisher Raman microscope DRX2xi at the H2P2 platform, University of Rennes (785 nm laser) or with a Horiba Xplora Plus Raman microscope, Paris Cité University (638 nm). The acquisition conditions are as follows:

- With the 785 nm laser on a ThermoFisher Raman microscope. Laser power 3.5 mW, exposure time 8s, 40 iterations, 40 iterations, pinhole diameter 50 μm, 400 lines/mm.
- With the 638 nm laser on Horiba Xplora Plus Raman microscope. Laser filter 0.1%, objective $\times$100, exposure time 5s, 10 accumulations, slit 200 μm, hole 500 μm, grating 600 (750 nm).

10 μL of slightly aggregated gold nanorods suspension through addition of pH=4 HCl solution (1 μL in 10 μL) were deposited onto a CaF_2 microscope slide to avoid the overlapping of self-fluorescence signal.

2.4 Computational setup

2.4.1 Density functional tight-binding (DFTB) details

First-principles calculations were performed using the self-consistent charge density functional tight-binding (SCC-DFTB) method as implemented in the version 22.2 of the DFTB+ program.[6] We used the *auorg* set of parameters[7] and its variation including phosphorous,[8] that allows for the description of gold-organics interactions. In all cases, a Becke-Johnson dispersion correction (D3) was included in the DFTB calculations. The electronic ground state was determined by minimizing the total energy of the system up to 10^{-5} Hartree. Γ-point calculations are performed for the large supercell containing the slab and the molecule, while the Brillouin zone is sampled using a Γ-centered $20\times20\times20$ Monkhorst-Pack for the gold bulk (*vide infra*).[9] Geometry optimizations are performed using a force criterion of 10^{-4} Hartree/Bohr. We compute the projected density of states (pDOS) with DFTB+ software and created the `.cube` files using the *waveplot* module of DFTB+. Resonant Raman spectra are obtained by using the mixed third derivatives of the energy with respect to electric field and positions to evaluate the variation of polarizability, hence the Raman activity of the system.[10] The configurations we used to simulate Raman spectra are described with their respective spectra in sections 3.5.2 and 3.5.3.

Calculating Raman intensities is cumbersome and requires approximations. In particular, we need to reduce the degrees of freedom of the system to limit the number of vibrational modes considered. In order to assess the impact of those approximations on the accuracy of our calculations, we study the case of a methyl molecule grafted on the Au(111) surface. Raman spectra are then calculated using different combinations of approximations. Finally, the best compromise between accuracy and calculation time is chosen. The approximations are:

- Reducing the amount of layers in the gold slab.
  - Removing the 3 innermost layers.
  - Removing the 2 innermost layers.
- Reducing the size of the Hessian matrix by freezing atoms
  - Freeze all atoms of the gold slab.
  - Freeze all atoms of the gold slab except the outermost layer.
  - Freeze all atoms of the gold slab except the ones bonding with the molecule.

Figure **S1** shows the calculated Raman spectra for the different systems. All sets of approximations are compared with the most expensive calculation in which all the layers of the gold slab are present and the full outermost layer is let free to move (grey line, Figure **S1**). We focus on the Au-C stretching mode (around

400 cm^{-1}) of particular interest in this work. Among all calculations, the best compromise is obtained when the two innermost layers are removed and only the Au atom bonding with the methyl is left free to move (red line in Figure **S1**). This scheme is used to compute Raman spectra for all other systems, including the mono- and tetra-podal calix[4]arenes on the gold structure. Figures **S22** and **S21** present the structures and corresponding Raman spectra presented in this work. We depict in orange the gold atoms that are let free to move, while the others are kept frozen. All atoms of the calix[4]arene are free to move.

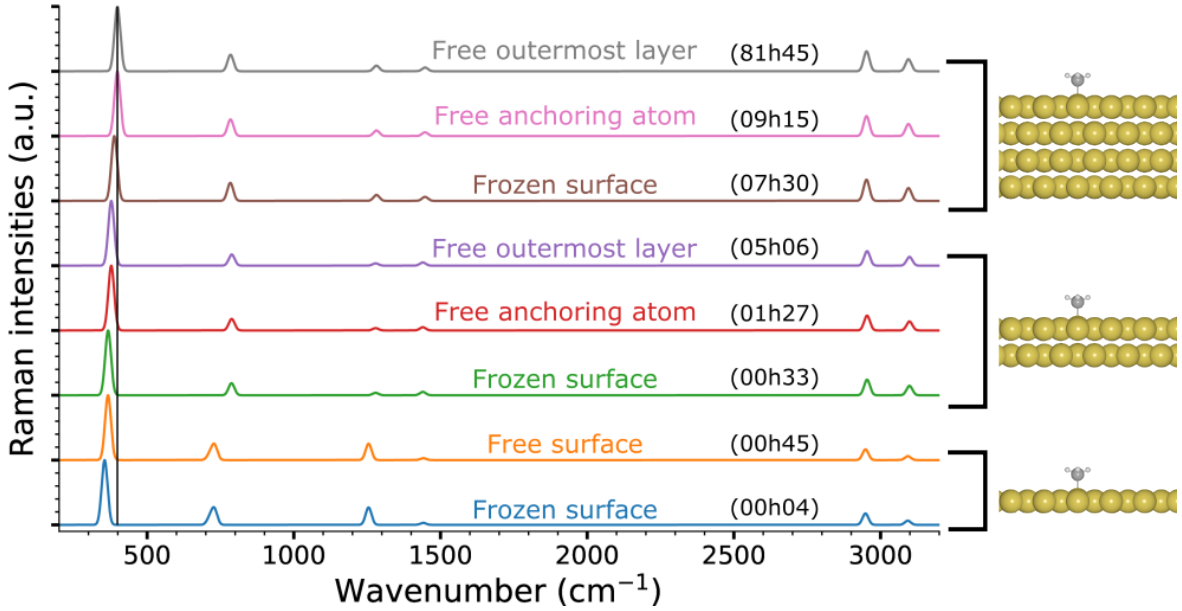

Figure S1 | Raman spectra of a methyl grafted to the Au(111) surface computed using different level of approximations. Structures are depicted on the right-hand side. In all cases, methyl atoms are free to move. Curves are labelled according to the gold atoms that are let free to move. We provide the total time of calculation in parenthesis. The black vertical line shows the position of the Au-C stretching mode for the reference calculation (gray line). The best compromise is obtained when the two innermost layers are removed and only the Au atom bonding with the methyl is left free to move (red line).

2.4.2 Gas phase calix[4]arene

Figure **S2** presents the gas phase groundstate geometry of the here-investigated calix[4]arene molecule. When dispersion corrections are introduced, it takes a parallelogram geometry at the large rim due to $\pi - \pi$ interactions between phenyl rings. Two opposite phenyl rings then are parallel to the vertical axis, while the two others form an angle of 63° with the vertical plane (52° without dispersion forces). Therefore, in the case of monopodal calix[4]arene, it creates two distinguishable anchoring sites that we labeled A and B. In addition, the calix[4]arene molecule shows a large rim of ∼0.44 or 0.65 nm^2 with and without dispersion forces, respectively. In figure **S2** the red and blue arrow measures the distance between two opposite hydrogen atoms that after departure leave a radical to form the anchoring sites.

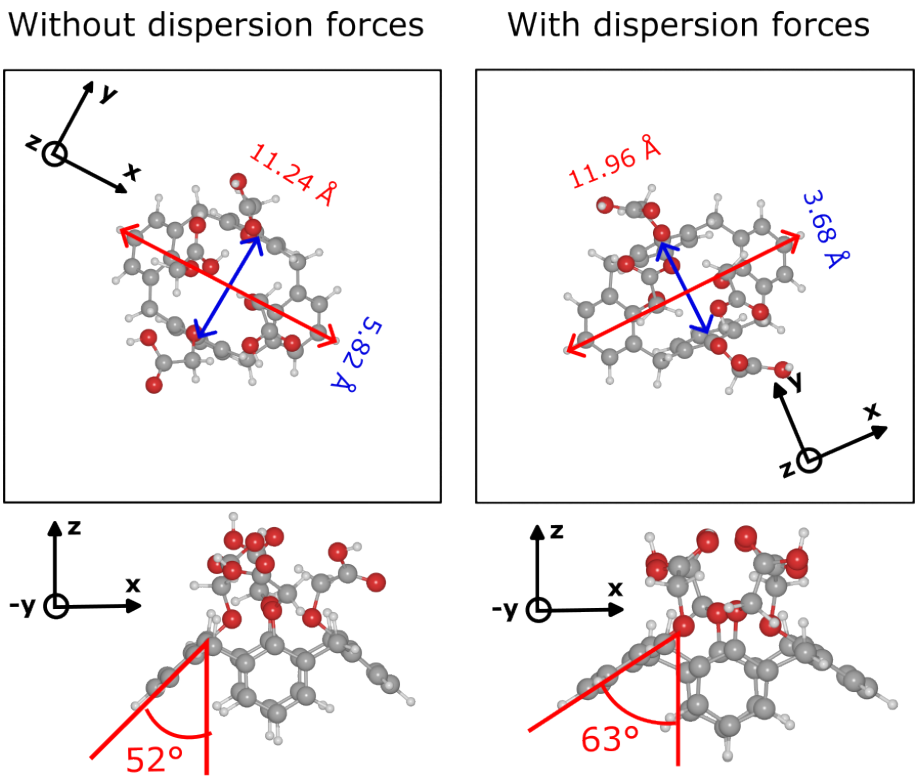

Figure S2 | Top and side view of the lowest energy configuration for the here-investigated calix[4]arene calculated using DFTB with and without D3 correction. Hydrogen, carbon and oxygen atoms are depicted by white, grey and red spheres, respectively. The black box represents the lateral extension of the simulation cell. The surface of the large rim of the calix[4]arene is ∼0.44 nm^2 when dispersion forces are considered.

2.4.3 Surface approximation for gold nanorods

Along their growth, nanorods present various facets with increasing areas (inset of Figure **S3**). It is worth noticing that, experimentally, the length of the gold nanorod is more than two orders of magnitude greater than the lateral size of the calix[4]arene. Hence, it can be approximated by an infinite nanowire.

Using the QuantumATK software,[11] we build nanowires of different diameters, and monitored the growth of the main plane along the [001] direction. Figure **S3** presents the variation of the length of the small and long sides with respect to the diameter of the gold nanowire. The increase appears to be linear. More importantly, a nanowire of a diameter greater than 20 nm, as experimentally used in this work, will present planes with a lateral extension greater than 7 nm, *i.e.* more than one order of magnitude the size of the calix[4]arene molecule.

Hence, the facets presented by the present nanorod are extremely large as compared to the size of the molecule and edge effects can be neglected. Therefore, to investigate the grafting of the molecule, we can use the most stable crystalline surface Au(111) to mimic the nanorod.

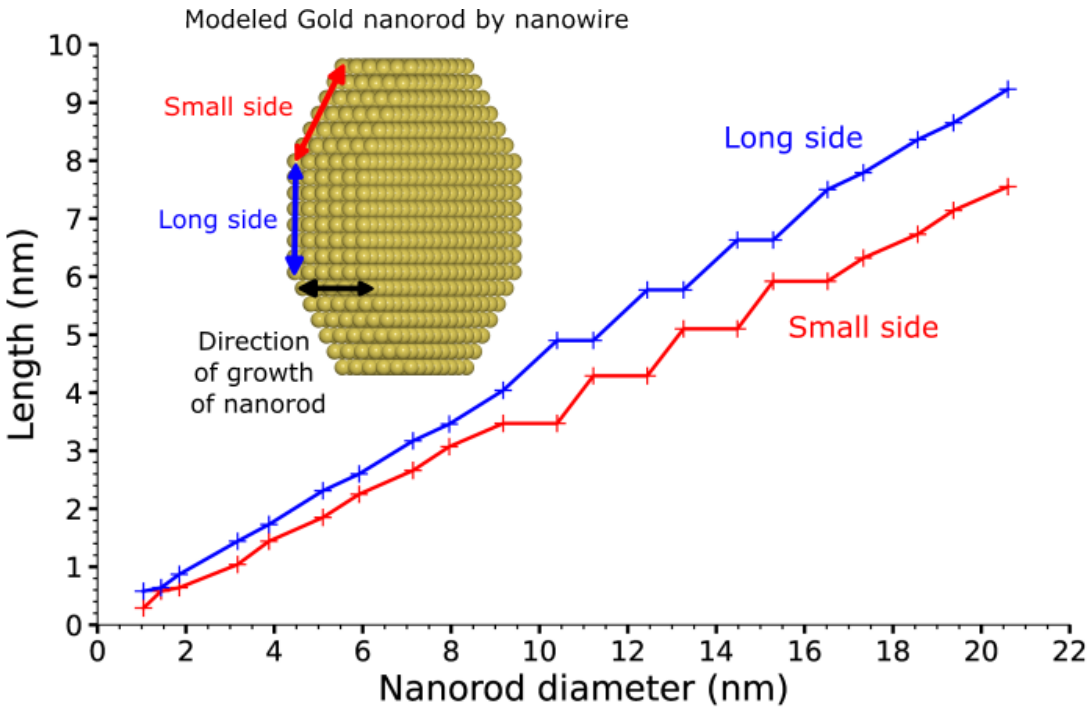

Figure S3 | Variation of the length of the long and small sides of the two planes for a gold nanowire as a function of its diameter. We observe that at 20 nm of diameter, the small side of the nanowire is 7 nm long, *i.e.* more than one order of magnitude greater than the lateral extension of the calix[4]arene. The inset represent a side view of the gold nanorod. Yellow spheres represent Au atoms.

2.4.4 Supported calix[4]arene on Au(111): configuration and anchoring sites

We approximate the grafting of calix[4]arene molecules on a gold nanorod by using the (111) surface of gold (*vide supra*).

The DFTB relaxed structure of bulk gold presents a lattice constant of a=4.05 Å, in excellent agreement with the experimental value, a=4.08 Å.[12] We then build a 4-layer slab of the $7 \times 4\sqrt{3}$ supercells, that allows to keep a nearly squared shape for the cell with a lateral size around 20 Å (Figure **S4**).

Along the geometry optimizations, the three outermost layers are free to move, while the lowest layer is kept frozen to emulate the gold bulk. We left 70.1 Å of vacuum between the slab and its images imposed by the periodic boundary conditions.

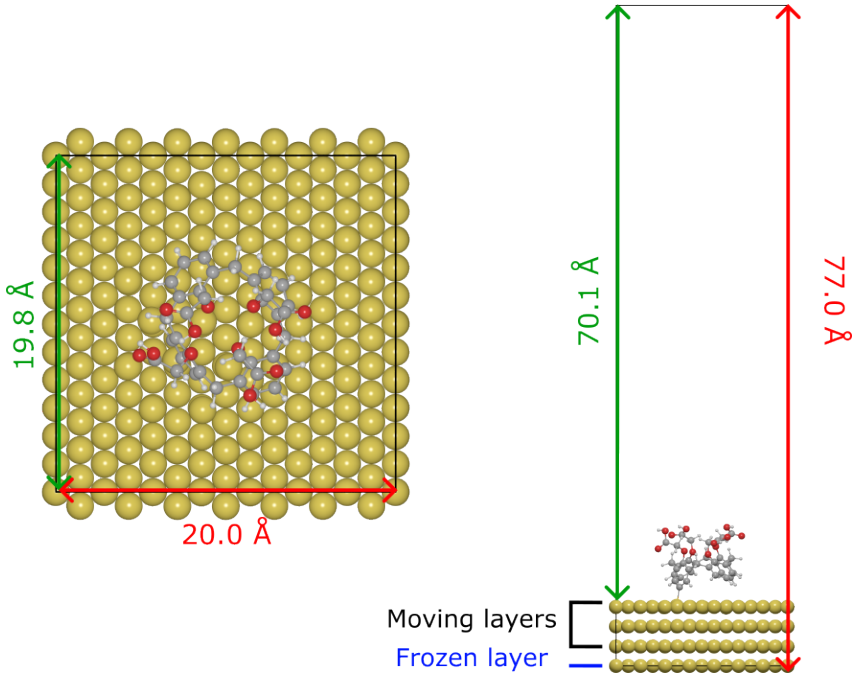

Figure S4 | Top and side view of the simulation box consisting of a 4-layer slab of the Au(111) surface and a calix[4]arene molecule. Along the geometry optimizations, the bottom layer of the gold slab is kept frozen, while the other atoms are free to move. White, grey, red and yellow spheres, are for hydrogen, carbon, oxygen and gold atoms, respectively.

The binding energy E_{binding} is defined as

$$E_{\text{binding}} = -E_{\text{adsorption}} = -\left(E_{\text{graft}} - \left(E_{\text{slab}} + E_{\text{vacuum}}\right)\right) , \tag{1}$$

where E_{graft}, E_{slab}, and E_{vacuum} are the energy of the molecule grafted on the Au(111) slab, the energy of the free Au(111) slab, and the energy of the molecule in vacuum, respectively.

3 Supplementary results

3.1 UV-Visible absorption spectroscopy of the gold nanorods suspension

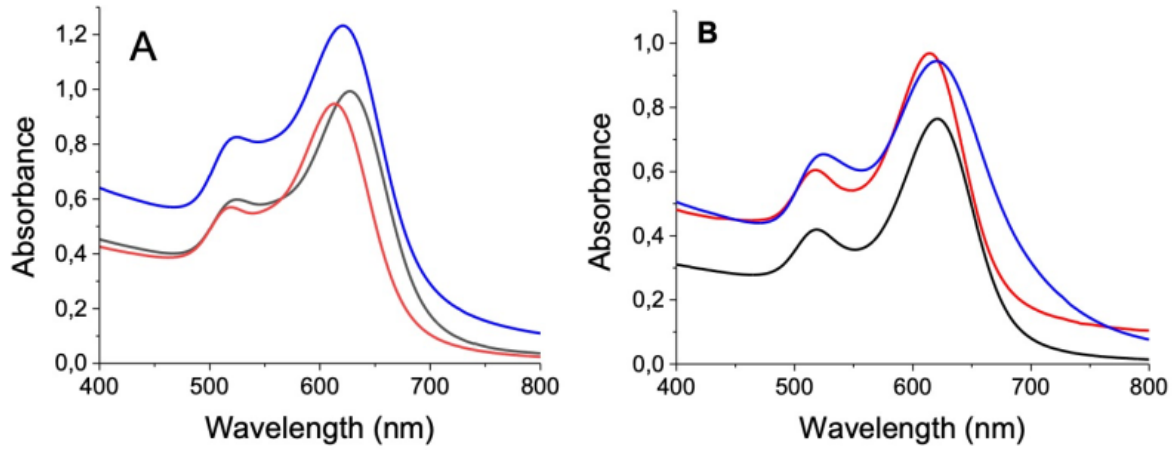

Figure S5 | UV-visible absorption spectra of gold nanorods aqueous suspension (A) Functionalization with $X_4(N_2^+)_4$, and (B) $X_4N_2^+$. Gold nanorods capped with CTAB (black line), addition of $NaBH_4$ and 40 min. stirring (red line), further addition of calix[4]arene molecules ($\sim 10^{-3}$ M) and overnight stirring (blue line).

3.2 Transmission electron microscopy

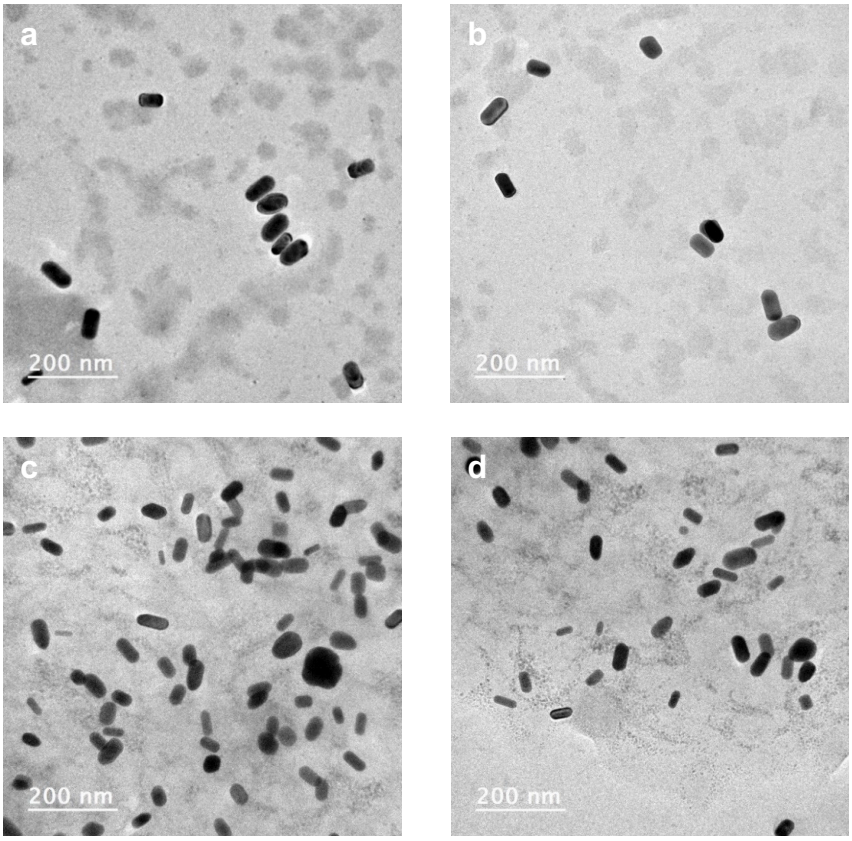

Figure S6 | TEM images of capped gold nanorods functionalized with (a-b) $X_4N_2^+$, and (c-d) $X_4(N_2^+)_4$.

Table S1 | Dimension analyses of gold nanorods.

Sample	Number of analysed particles	Length (nm)	Width (nm)	AR
CTAB AuNRs	130	62.1±6.0	27.7±3.8	2.2±0.5
Monopodal AuNRs	72	62.6±6.6	24.3±3.6	2.6±0.6
Tetrapodal AuNRs	93	59.1±5.9	24.6±3.3	2.4±0.6

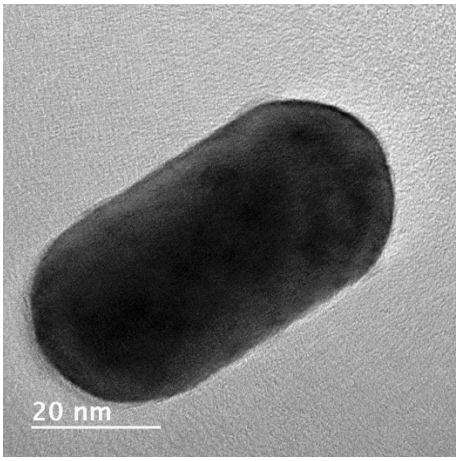

Figure S7 | TEM image of a single nanorod capped with CTAB.

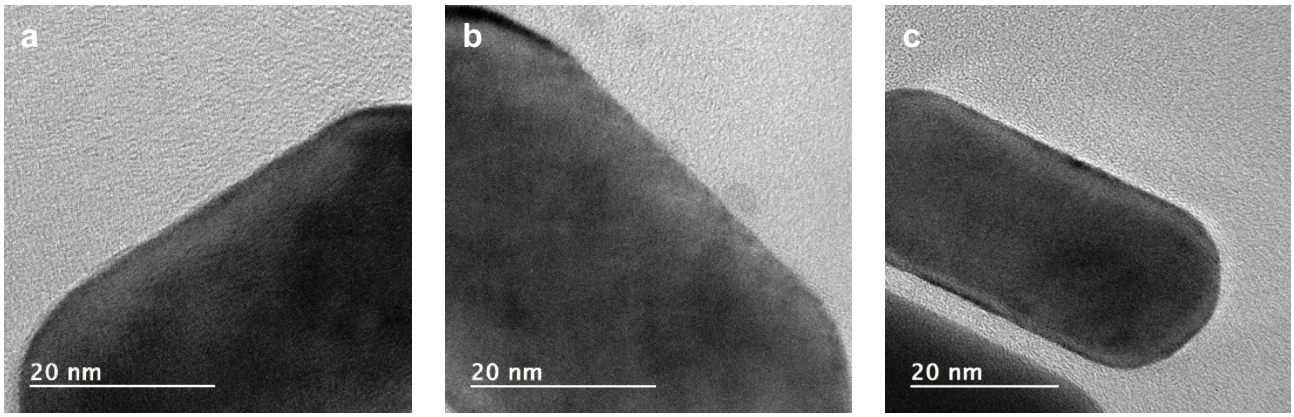

Figure S8 | HRTEM images of single nanorods capped (a) with CTAB, (b) from $X_4N_2^+$, and (c) $X_4(N_2^+)_4$.

3.3 XPS survey spectra

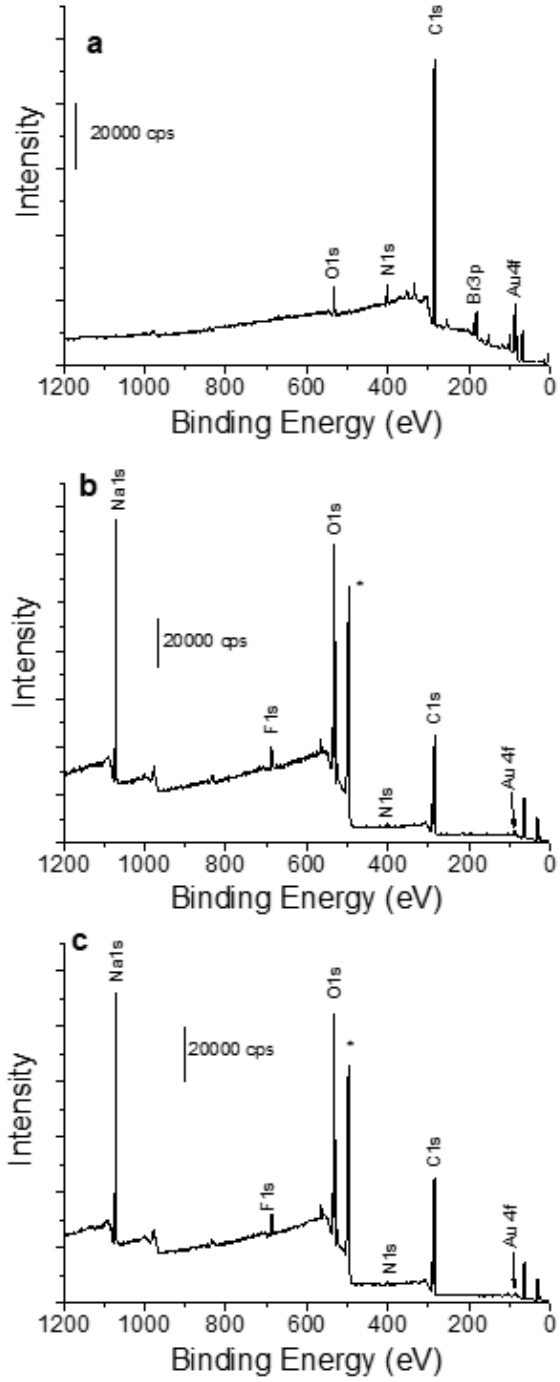

Figure S9 | Survey spectra of a deposit onto silicon substrate of (a) gold nanorods capped with CTAB, (b) coated from $X_4N_2^+$, and (c) $X_4(N_2^+)_4$. * is Na Auger peak.

3.4 Calix[4]arene anchoring

The presence of two sites A and B (*vide supra*), creates two regioisomers when investigating the grafting of the mono-podal calix[4]arene. Similarly, in the case of the double and triple-podal molecules several configurations have to be considered. Therefore, in Figure **S10** we present the side view of all the different conformers studied for Au(111). Then, in Figs **S11**, **S12** and **S13** we present the mono and tetrapodal configurations of calix[4]arene on Au(100), Au(110) and Au(520), respectively. For the monopodal, except for Au(520), we observe that the molecule is anchored on distinct, but equivalent, top sites. The distance between the binding Au and C atoms, as well as the distance between the center of mass of the calix[4]arene and the slab are given in Table **S2**. We observe that the C atom is at $\sim$3.5 Å from the surface when unbound, and at $\sim$2.2 Å when bound.

The computed total energy of all the different conformers and regioisomers are provided in Table **S3**. Figure **S14** compares for the Au(111) surface the energies for (i) the DFTB level of theory,[7,13,14] and (ii) density functional theory (PBE+D3 functional with VASP software).[15,16] We observe an excellent agreement between DFTB+D3 and PBE+D3 levels of theory. DFTB calculations without including D3 corrections provide adsorption energies higher by almost 1 eV. Interestingly, the binding energy (Figure **S15**) diminishes as we increase the number of anchors from 1 to 4, by 0.9, 1.2, 1.6 and 1.5 eV for Au(111), Au(100), Au(110) and Au(520), respectively.

Table S2 | Distances between the anchoring carbons of the phenyls and the anchoring Au site (d_{Au-C}), and between the center of mass of the calix[4]arene molecule and the outermost layer of the slab ($d_{Calix-Slab}$) computed for each configuration presented Figure **S10** for Au(111). The most important configuration of the other facet are represented on figures **S11**, **S12** and **S13**. The C atom is at ∼3.5 Å from the surface when unbound, and at ∼2.2 Å when bound. For one case, $d_{Au-C} > 3.5$ due to the inclination of the calix[4]arene on the slab.

Surface index	(111)					(100)					(110)					(520)				
Label	d_{Au-C} (Å)				$d_{Calix-Slab}$ (Å)	d_{Au-C} (Å)				$d_{Calix-Slab}$ (Å)	d_{Au-C} (Å)				$d_{Calix-Slab}$ (Å)	d_{Au-C} (Å)				$d_{Calix-Slab}$ (Å)
Physisorbed	3.45	3.54	3.54	3.54	6.11	3.99	6.28	3.93	3.57	6.71	3.36	3.30	3.16	3.18	5.87	3.54	3.54	3.53	3.76	5.80
1 Anchor-A	2.22	3.61	3.54	3.63	5.95	2.20	3.61	3.86	3.54	5.83	2.18	3.24	3.13	3.34	5.55	2.16	3.54	3.54	3.60	5.58
1 Anchor-B	3.54	2.21	3.57	3.54	5.87	3.86	2.20	3.64	3.54	6.03	3.23	2.20	3.54	3.19	5.64	3.27	2.16	3.68	3.54	5.73
2 Anchors-A	2.24	2.22	3.55	3.59	5.73	2.23	2.23	3.54	3.37	5.74	2.20	2.21	3.35	3.40	5.64	2.15	2.19	3.25	3.82	5.44
2 Anchors-B	2.23	3.54	2.23	3.54	5.74	2.24	3.25	2.24	3.24	5.53	2.18	3.54	2.18	3.34	5.53	3.54	2.19	3.33	2.21	5.36
2 Anchors-C	3.54	2.23	3.46	2.23	5.59	3.24	2.24	3.25	2.24	5.65	3.40	2.18	3.34	2.18	5.54	2.18	3.54	2.20	3.54	5.27
3 Anchors-A	2.24	2.22	2.23	3.62	5.57	2.23	2.23	2.24	3.24	5.46	2.20	2.22	2.18	3.38	5.50	2.17	2.19	3.35	2.21	5.33
3 Anchors-B	3.54	2.23	2.22	2.23	5.60	3.25	2.23	2.22	2.24	5.41	3.40	2.18	2.22	2.18	5.47	2.15	2.21	2.19	3.35	5.20
4 Anchors	2.24	2.24	2.22	2.21	5.49	2.23	2.23	2.22	2.22	5.38	2.20	2.20	2.20	2.20	5.49	2.17	2.18	2.21	2.21	5.18

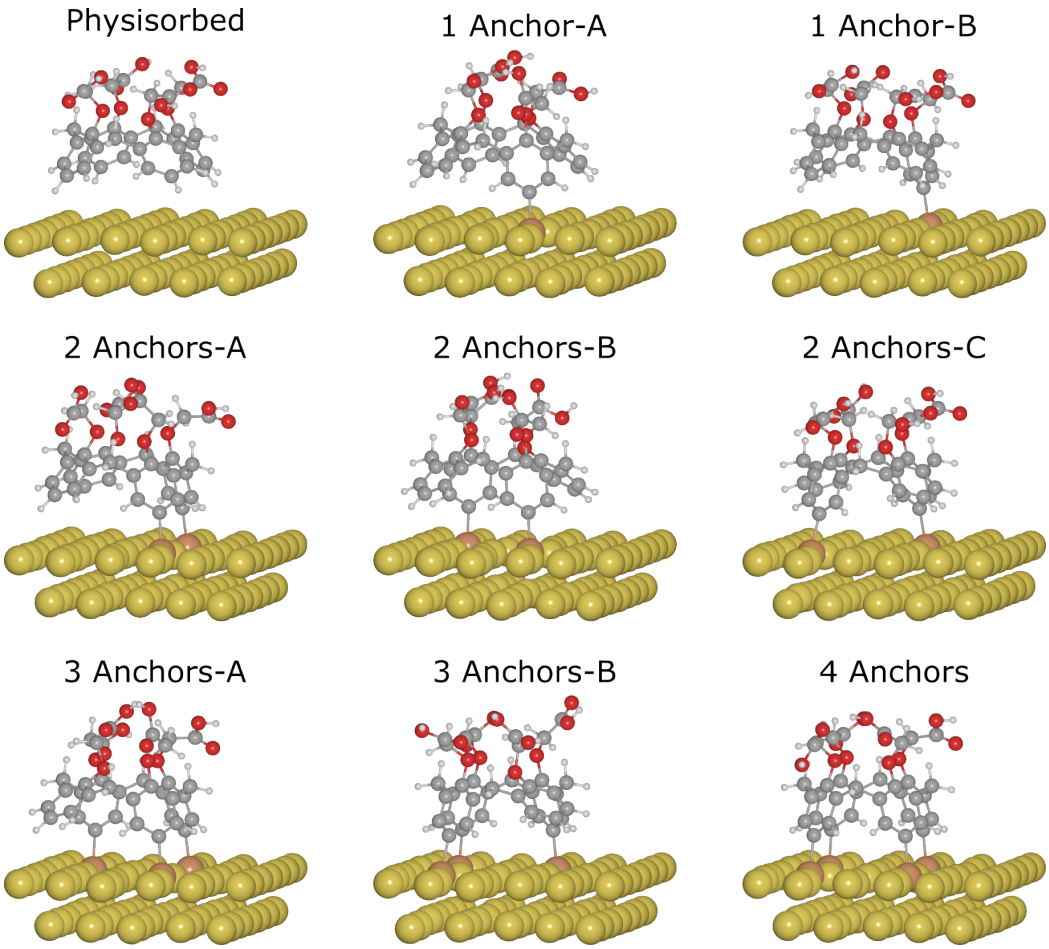

Figure S10 | Side view of the lowest energy configurations for calix[4]arene grafted on Au(111) computed at DFTB+D3 level of theory. White, grey, red and yellow spheres are hydrogen, carbon, oxygen and gold atoms. The orange atoms are the Au atoms bonding with the calix[4]arene.

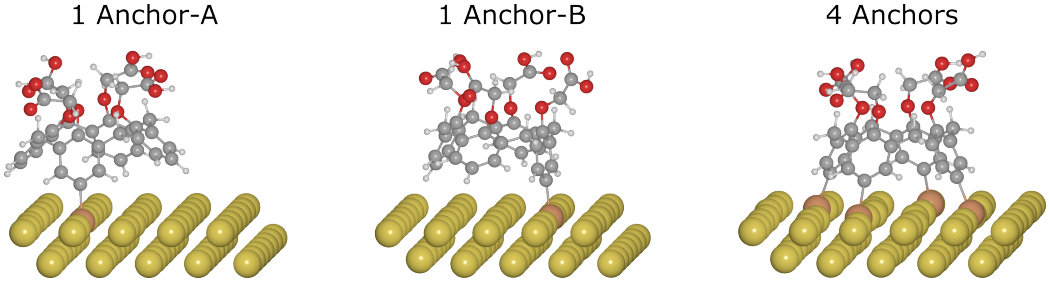

Figure S11 | Side view of the lowest energy configurations for mono and tetrapodals calix[4]arene grafted on Au(100) computed at DFTB+D3 level of theory. Here we depict only the configuration for which Raman spectrum has been simulated. White, grey, red and yellow spheres are hydrogen, carbon, oxygen and gold atoms. The orange atoms are the Au atoms bonding with the calix[4]arene.

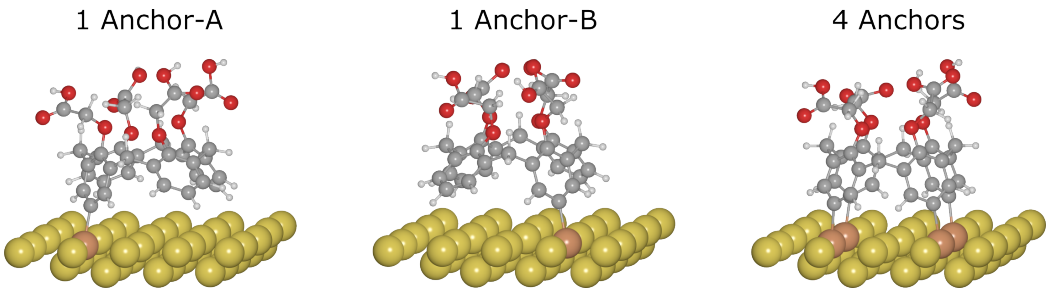

Figure S12 | Side view of the lowest energy configurations for mono and tetrapodals calix[4]arene grafted on Au(110) computed at DFTB+D3 level of theory. Here we depict only the configuration for which Raman spectrum has been simulated. White, grey, red and yellow spheres are hydrogen, carbon, oxygen and gold atoms. The orange atoms are the Au atoms bonding with the calix[4]arene.

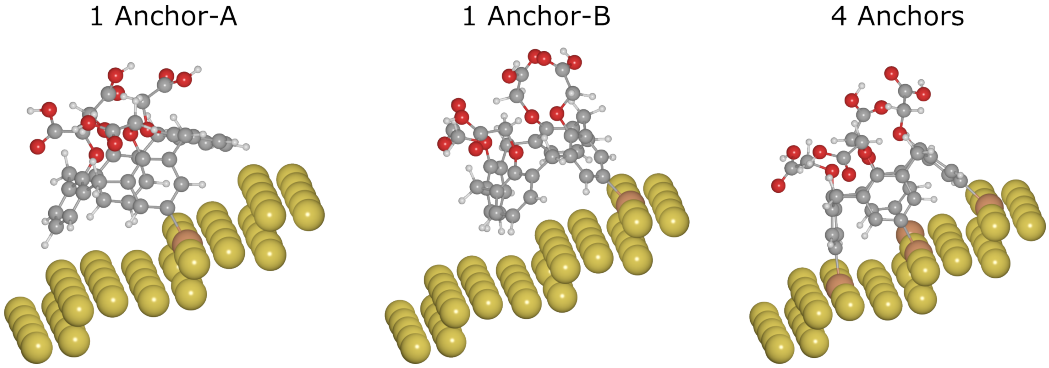

Figure S13 | Side view of the lowest energy configurations for mono and tetrapodals calix[4]arene grafted on Au(520) computed at DFTB+D3 level of theory. Here we depict only the configuration for which Raman spectrum has been simulated. White, grey, red and yellow spheres are hydrogen, carbon, oxygen and gold atoms. The orange atoms are the Au atoms bonding with the calix[4]arene.

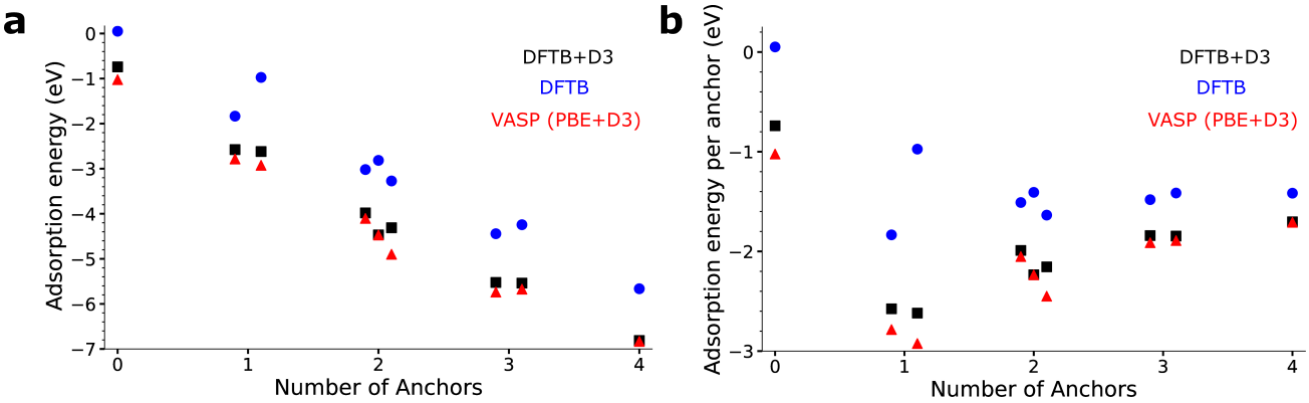

Figure S14 | Comparison of the adsorption energies and adsorption energies per anchor of the Au(111) surface, computed using DFTB with dispersion corrections (black squares), without dispersion corrections (blue circles), and DFT with the GGA functional PBE and dispersion corrections D3 as implemented in the VASP code (red triangles). We observe that as we are increasing the number of bonds, we are stabilizing the system by increasing the binding energy. On the other hand, the energy per anchor is decreasing by 0.9 eV as we increase the number of bond from 1 to 4 bounds.

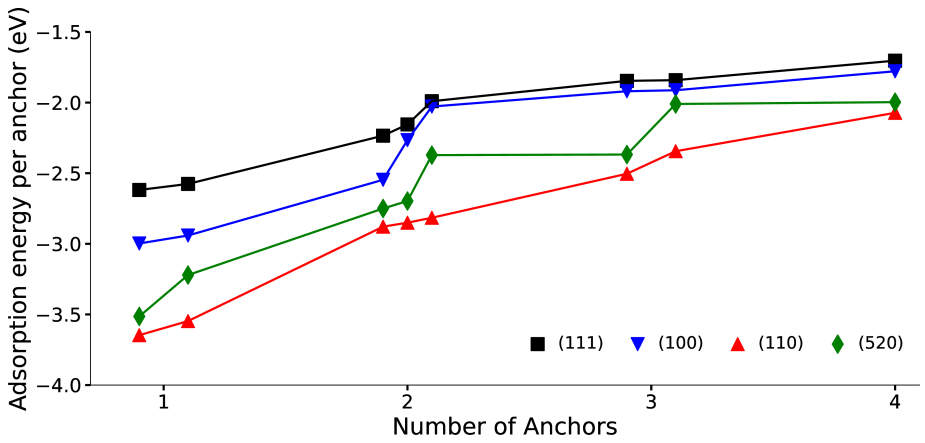

Figure S15 | DFTB adsorption energies of calix[4]arene on Au(100), Au(110), Au(111), and Au(520) surfaces as a function of the number of anchors. We observe that the energy per anchor is decreasing by 1.2 eV, 1.6 eV, 0.9 eV and 1.5 eV as we increase the number of bond from 1 to 4 bounds, for Au(100), Au(110), Au(111), and Au(520), respectively.

Table S3 | Adsorption energies computed at DFTB+D3 level of theory. Labels refer to Figures **S10**, **S11**, **S12** and **S13**.

Label	Number of anchors	Energy (eV)				Energy per anchor (eV)			
Surface index		(111)	(100)	(110)	(520)	(111)	(100)	(110)	(520)
Physisorbed	0	-0.740	-1.209	-1.201	-1.244	-0.740	-1.209	-1.201	-1.244
1 Anchor-A	1	-2.576	-2.941	-3.547	-3.221	-2.576	-2.941	-3.547	-3.221
1 Anchor-B	1	-2.619	-2.997	-3.647	-3.514	-2.619	-2.997	-3.647	-3.514
2 Anchors-A	2	-3.981	-3.840	-5.757	-5.393	-1.990	-1.920	-2.878	-2.697
2 Anchors-B	2	-4.469	-4.531	-5.701	-4.737	-2.234	-2.266	-2.850	-2.368
2 Anchors-C	2	-4.310	-5.093	-5.631	-5.500	-2.155	-2.547	-2.816	-2.750
3 Anchors-A	3	-5.524	-5.738	-7.512	-6.029	-1.841	-1.913	-2.504	-2.010
3 Anchors-B	3	-5.539	-6.085	-7.033	-7.115	-1.846	-2.028	-2.344	-2.372
4 Anchors	4	-6.813	-7.113	-8.290	-7.988	-1.703	-1.778	-2.073	-1.997

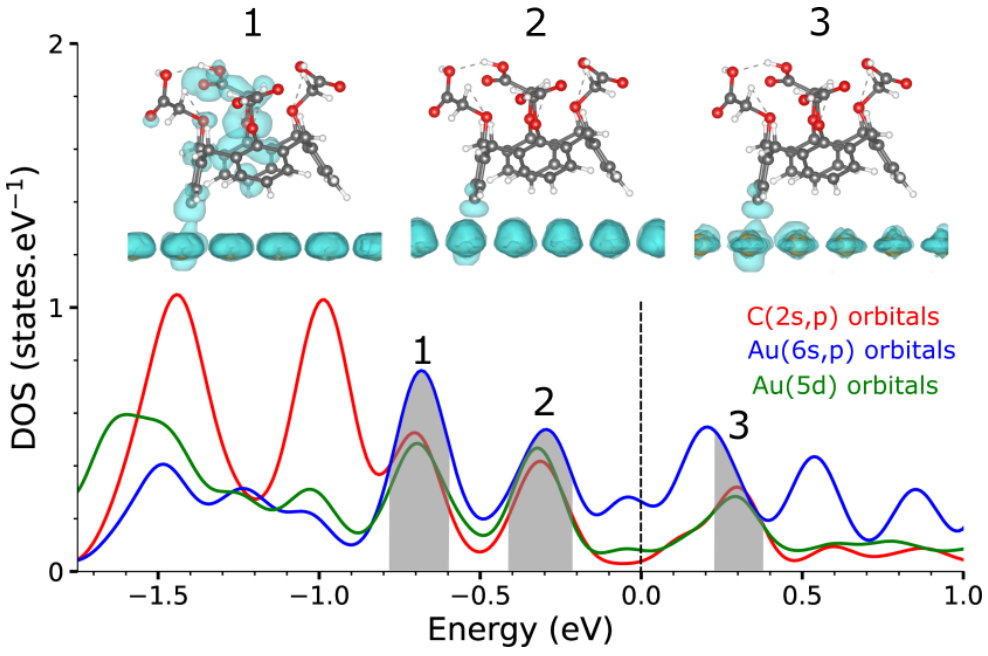

Figure S16 | Density of states (DOS) projected on C(2s,2p), Au(6s,6p) and Au(5d) orbitals for one monopodal calix[4]arene system grafted on Au(111). Energies have been shifted so the Fermi level is at 0. Insets show the charge densities integrated over the corresponding energetic windows depicted in grey.

3.5 Raman spectroscopy

3.5.1 Additional experimental Raman spectra

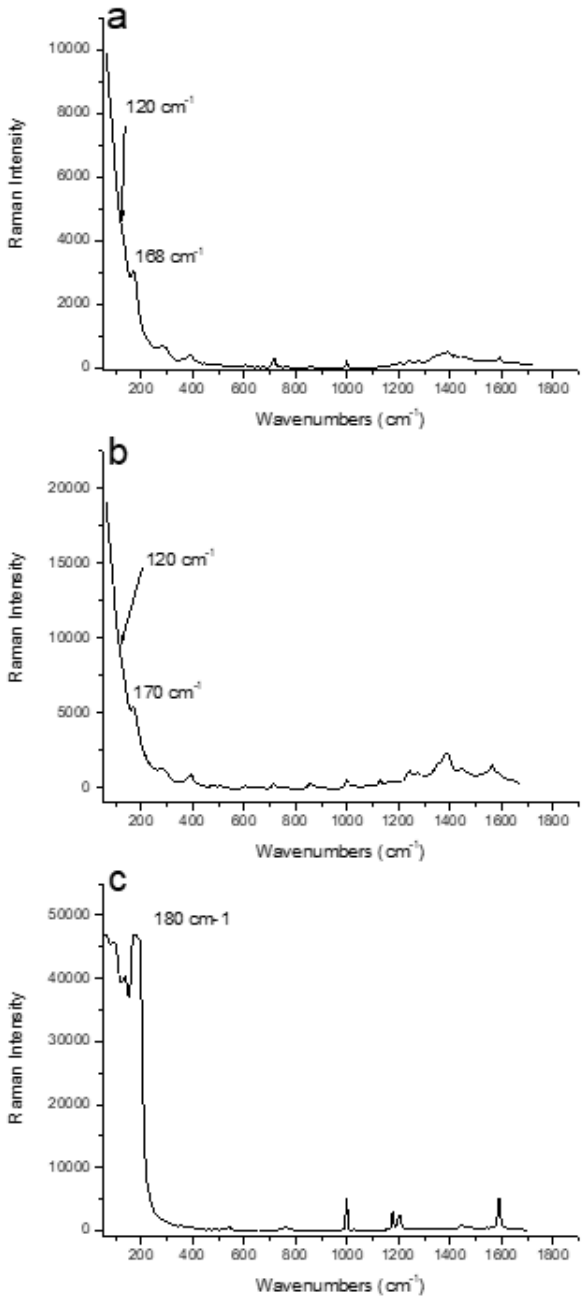

Figure S17 | Experimental Raman spectra (785 nm laser) of gold nanorods coated by (a) mono-, (b) tetrapodal calixarenes, and (c) CTAB molecules.

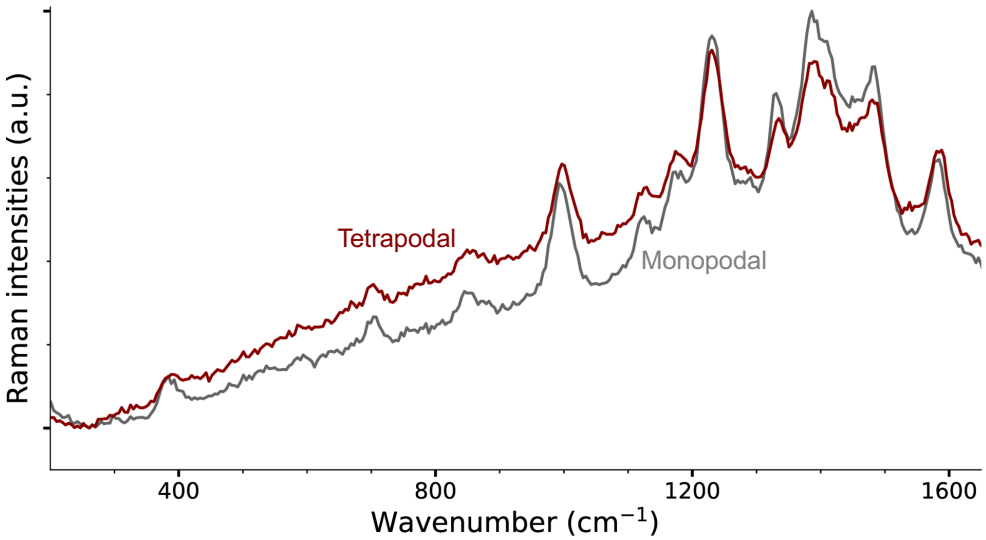

Figure S18 | Raman spectra of gold nanorods modified from the grafting of $X_4N_2^+$ (grey line) and $X_4(N_2^+)_4$ diazonium (red line) recorded with a laser at 638 nm.

3.5.2 DFTB description of Au complexes

Figure **S19** presents the ground-state geometries of the gold complexes for which we computed Raman spectra (Figure **S20**). Table **S4** details the assignment of several important modes.

In those complexes, the Au-C stretching mode is comprised between 200-550 cm^{-1}. Importantly, the Au-C stretching mode is shifted by hundreds of cm^{-1} depending on the gold complex. In the case of the linear $AuCN_2^-$, it is located at 428 cm^{-1}, while for $MeAuPMe_3$ it appears at 546 cm^{-1} (see main text). Furthermore, in $PhAuPMe_3$ complex, where Me is substituted by a Ph group, the Au-C stretching is displaced to 248 cm^{-1}, *i.e.* 300 cm^{-1} downshifted. In the case of the acac ligand, we failed to clearly identify one Au-C stretching mode, however the deformation of the acac ligand leads to variation of the Au-C distance, hence the value noted Table **S4**.

The peak situated at 2200 cm^{-1} for $AuCN_2^-$ corresponds to the C≡N stretching. The two peaks situated between 1450-1500 cm^{-1} for $MeAuPMe_3$ and Me_3AuPMe_3 complexes correspond to Me deformations. The phenyl stretching modes of $PhAuPMe_3$ and Ph_3AuPMe_3 described in the main text are shown with triangles in Figure **S20** and labeled $\nu_{C=C,E_{1u}}$ and $\nu_{C=C,E_{2g}}$ in Table **S4**. The peaks located between 1600-1700 cm^{-1}, for both acac complexes, are stretching of C=O bond from the acac ligand. In the acac spectrum it has not been possible to clearly assign the modes since they are essentially composed of several modes of low intensities.

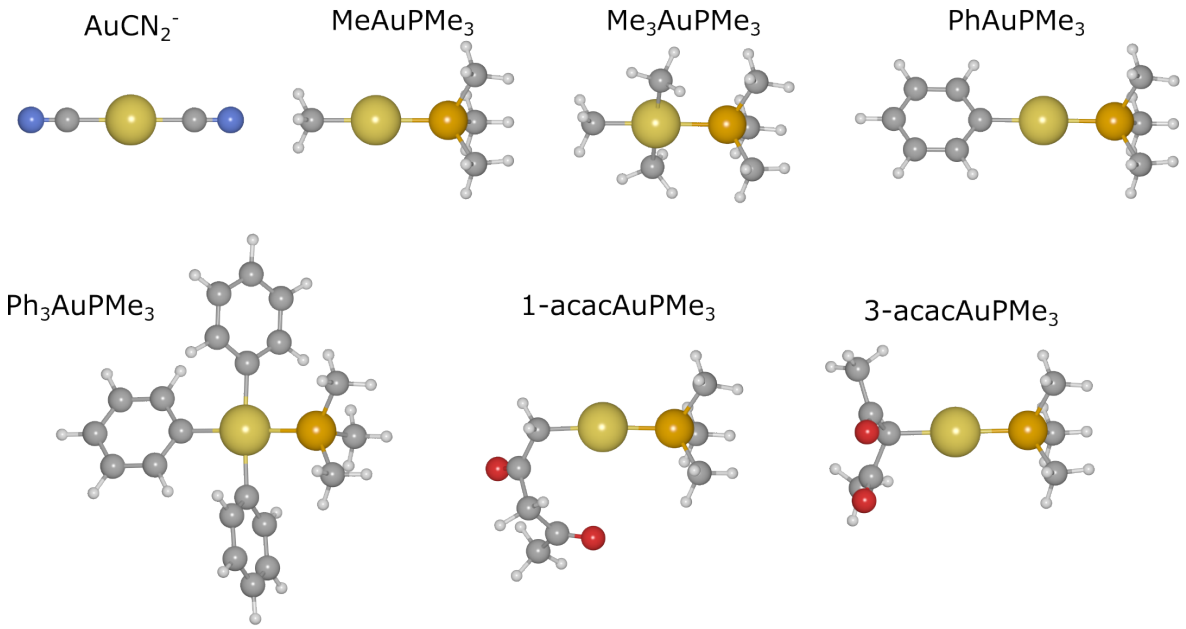

Figure S19 | Gold complexes used in this work. White, grey, red, blue, orange and yellow spheres, are for hydrogen, carbon, oxygen, nitrogen, phosphorus and gold atoms, respectively

Table S4 | Computed Raman-active vibration modes (in cm^{-1}) of gold complexes with qualitative assignments. When available, the experimental reference is provided in brackets.

Vibration	$Au(CN)_2^-$	$MeAuPMe_3$	Me_3AuPMe_3	$PhAuPMe_3$	Ph_3AuPMe_3	1-acac$AuPMe_3$	3-acac$AuPMe_3$
$\nu_{Au\text{-}C}$	428 (427[17])	546 (535[18])	513, 543 (512, 540[18])	248	213, 230, 252	(330, 338[17])	(330, 338[17])
$\nu_{C=C,E_{1u}}$				1461, 1560	1457, 1464		
					1543, 1544, 1545		
					1584, 1587, 1589		
$\nu_{C=C,E_{2g}}$				1784, 1821	1782, 1783, 1784		
					1810, 1813, 1814		
C≡N stretching	2200						
Me lig. deformation		1450-1500	1450-1500			1450-1470	1450-1470
PMe_3 umbrella + $\nu_{Au\text{-}P}$		404, 700	396, 701	406, 701	401, 700	411, 704	412, 703
		720	729, 730	722, 723	732, 736	725, 727	725, 726
acac deformation						510, 704	287, 449
							637, 679
acac lig. $\nu_{C=O}$						1729, 1751	1734, 1788

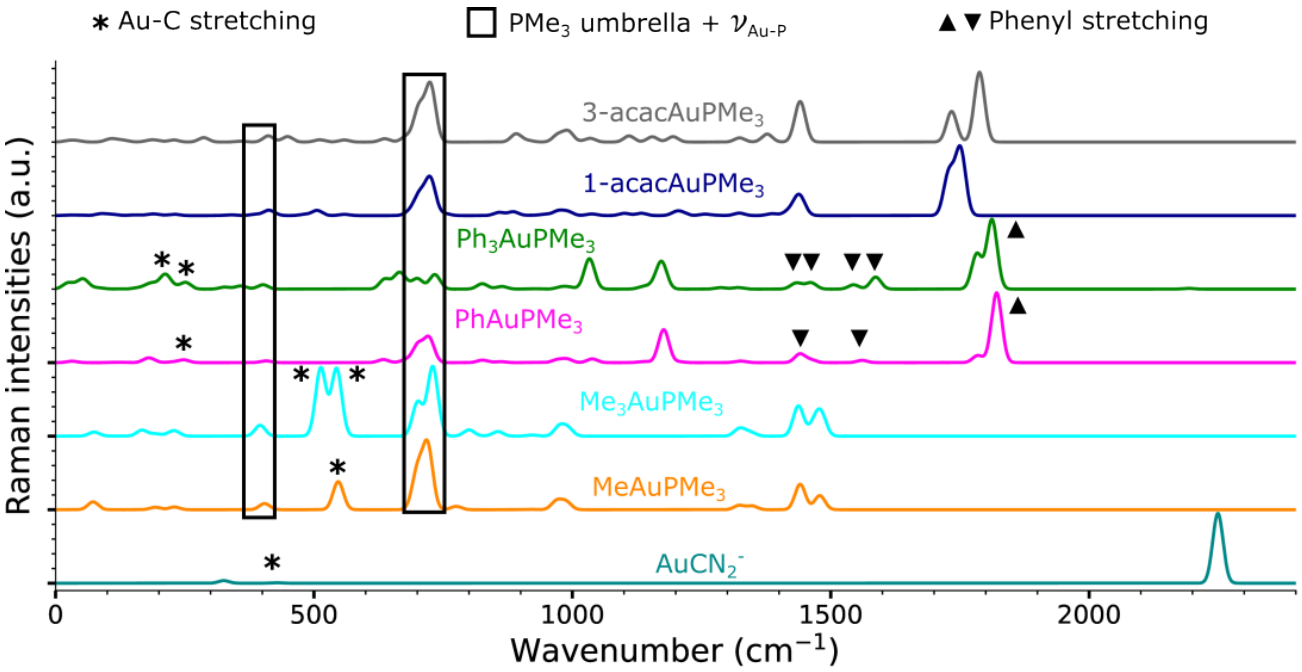

Figure S20 | DFTB computed Raman spectra for various gold complexes. The peaks identified by symbols are described in the main text. The Au-C stretching mode is comprised between 200-550 cm^{-1} depending on the gold complex. By substituting Me by Ph in gold complex, the Au-C stretching mode is downshifted by 300 cm^{-1}.

3.5.3 DFTB description of organic molecules adsorbed on Au(111)

Figure **S21** presents the simulated Raman spectra for organic molecules grafted on Au(111), as well as $MeAuPMe_3$ gold complex for comparison. Each system is depicted in Figure **S22**. In Figure **S21**, we marked the peaks that are described in the main text with the same nomenclature. By grafting the Me on Au(111) the Au-C stretching mode is downshifted with respect to the gold complex. Then, by substituting Me by Ph, the mode is again downshifted, resulting in a Au-C stretching mode at 218 cm^{-1}, *i.e.* 330 cm^{-1} downshifted comparing to $MeAuPMe_3$.

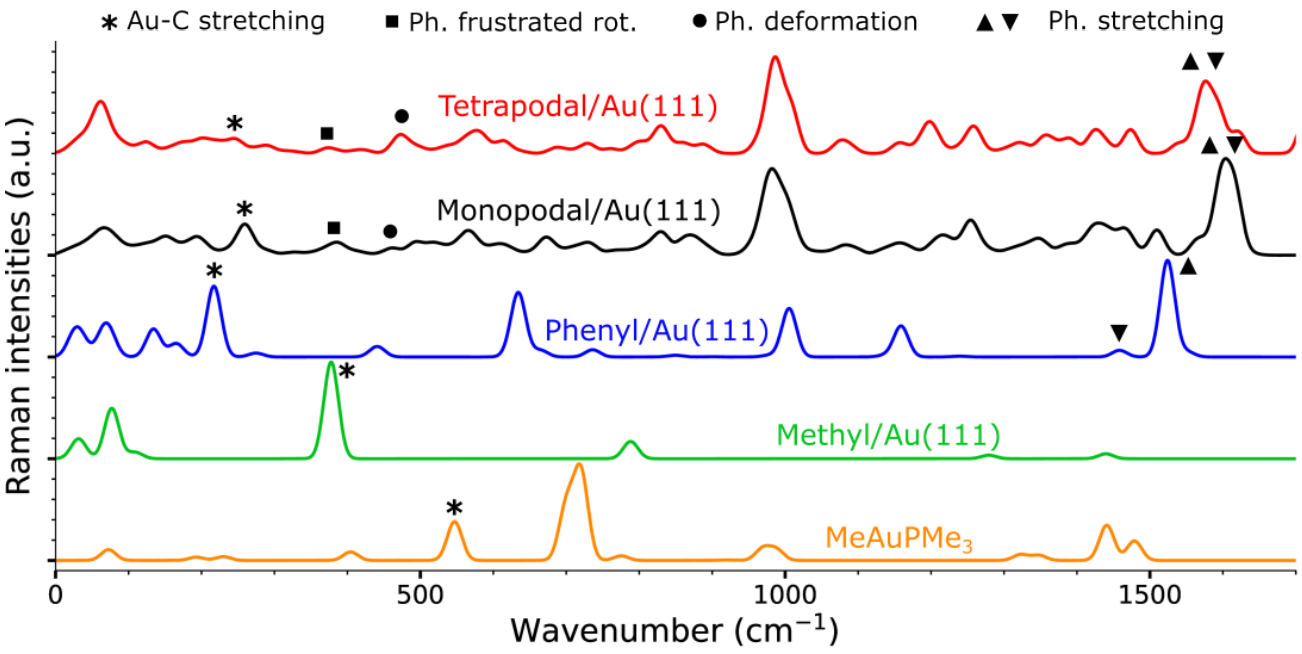

Figure S21 | DFTB computed Raman spectra for organic molecules adsorbed on Au(111) surface. The Au-C stretching mode is downshifted by 330 cm^{-1} when going from a Me in gold complex to a Ph grafted on Au(111). We also observe a shift of the Ph stretching modes at frequencies above 1500 cm^{-1} depending on Ph surrounding.

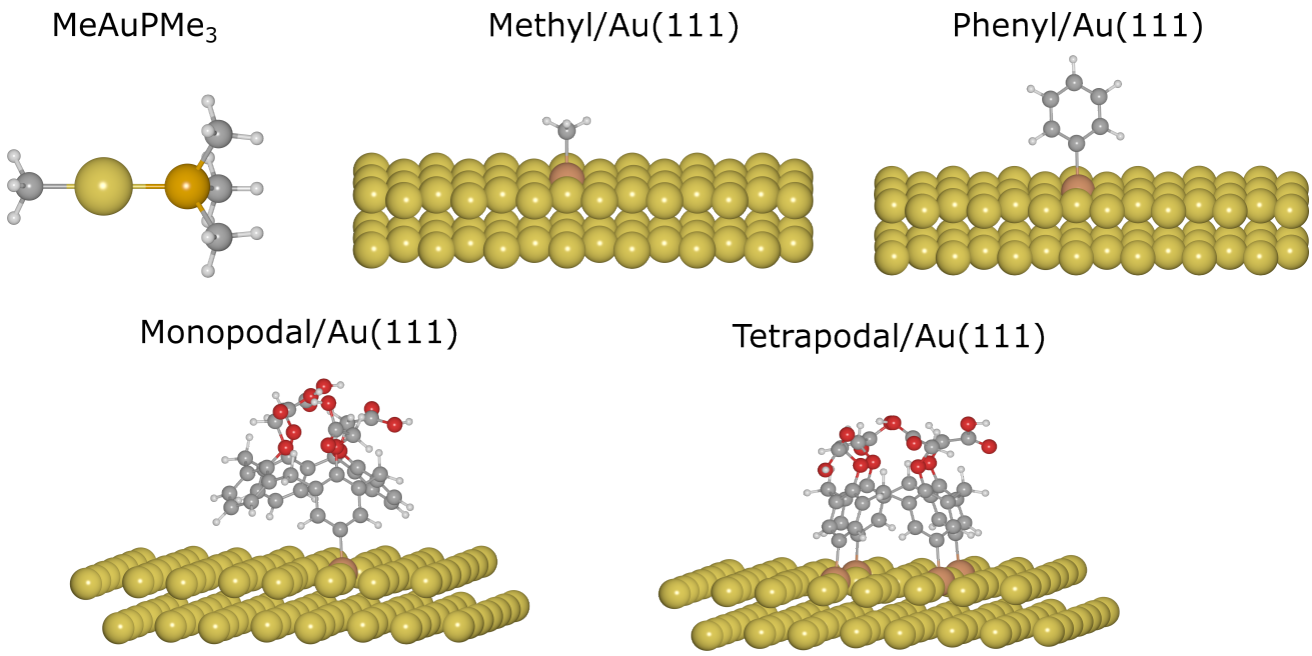

Figure S22 | Structures of the system considered in this work. White, grey, red, blue, orange and yellow spheres, are for hydrogen, carbon, nitrogen, oxygen, phosphorus and gold atoms, respectively. The atoms in orange in the slab represent the gold atoms to which the molecule is bonding.

3.5.4 DFTB description of calix[4]arene adsorbed on selected gold facets

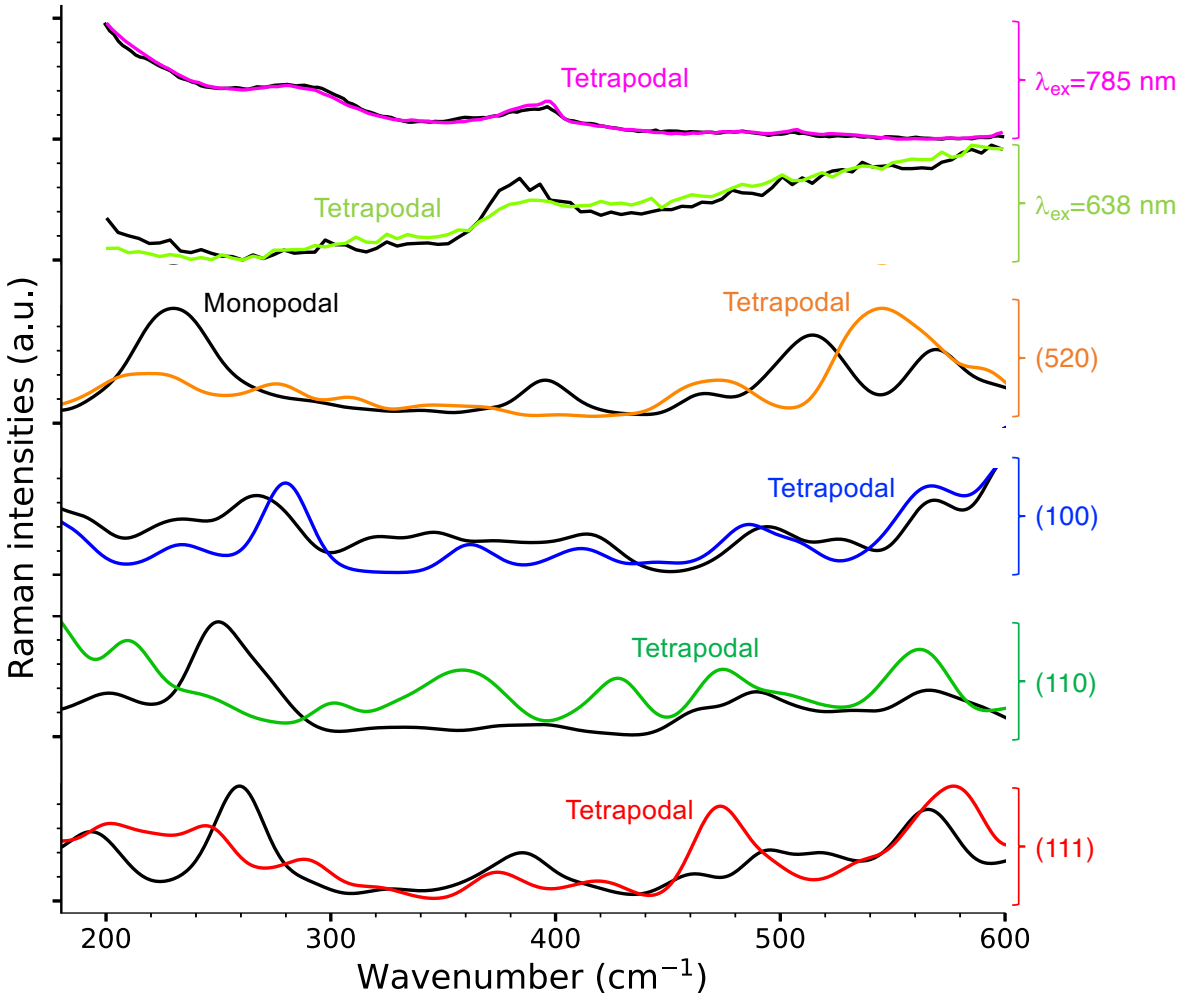

Figure S23 | Experimental Raman spectra between 200 and 550 cm^{-1} of gold nanorods coated from the grafting of $X_4N_2^+$ and $X_4(N_2^+)_4$ recorded with a laser at 785 and 638 nm, and simulated spectra for the monopodal and tetrapodal calix[4]arene grafted on Au (111), (110), (100) and (520) facets. For each facet, the signal of the monopodal is depicted in black line, while color lines are used for the tetrapodal systems.

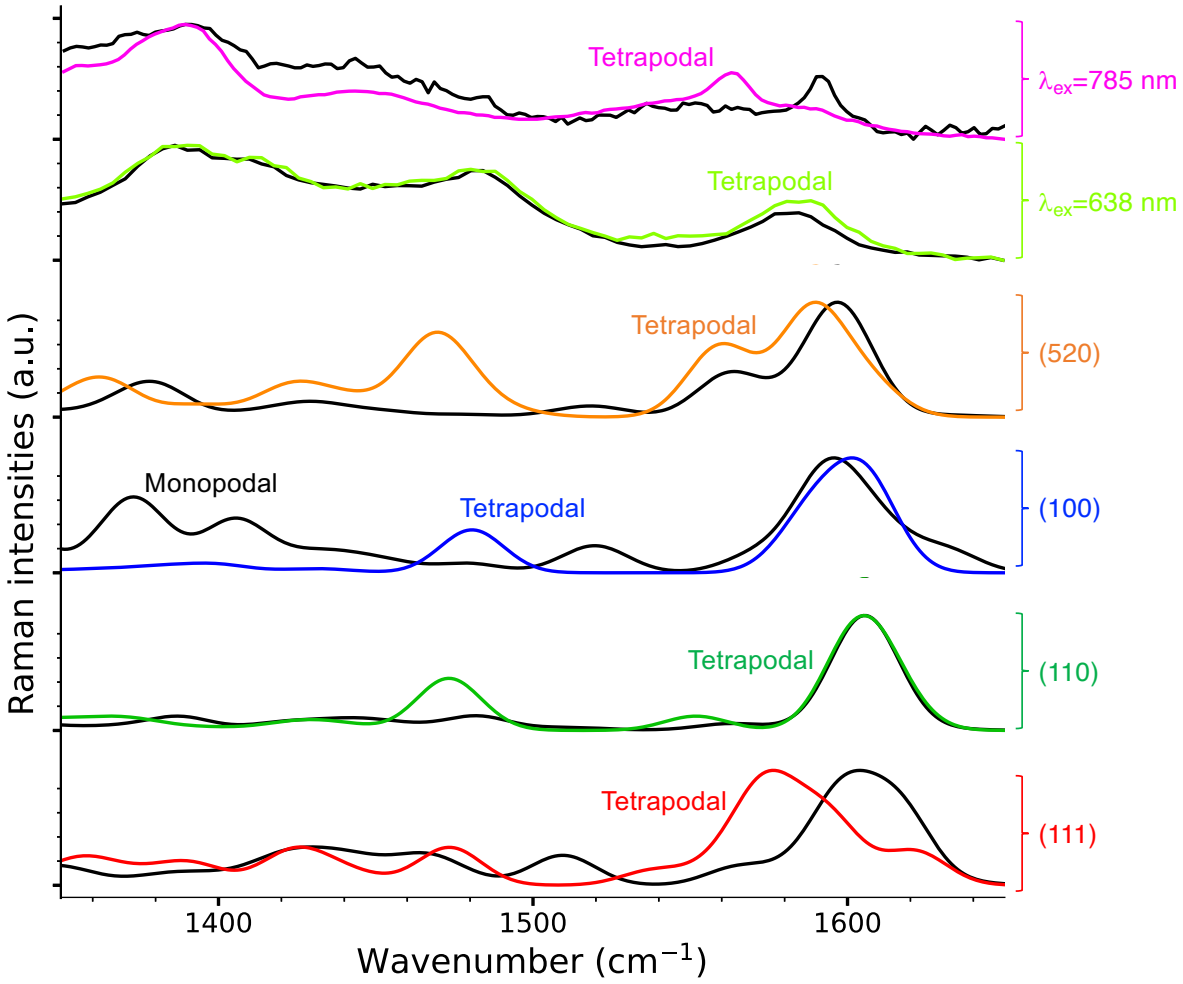

Figure S24 | Experimental Raman spectra between 1400 and 1600 cm^{-1} of gold nanorods coated from the grafting of $X_4N_2^+$ and $X_4(N_2^+)_4$ recorded with a laser at 785 and 638 nm, and simulated spectra for the monopodal and tetrapodal calix[4]arene grafted on Au (111), (110), (100) and (520) facets. For each facet, the signal of the monopodal is depicted in black line, while color lines are used for the tetrapodal systems.

References

[1] Mattiuzzi, A., Jabin, I., Mangeney, C., Roux, C., Reinaud, O., Santos, L., Bergamini, J.-F., Hapiot, P. & Lagrost, C. Electrografting of calix[4]arenediazonium salts to form versatile robust platforms for spatially controlled surface functionalization. *Nat. Commun.* **3**, 1130 (2012).

[2] Santos, L., Mattiuzzi, A., Jabin, I., Vandencasteele, N., Reniers, F., Reinaud, O., Hapiot, P., Lhenry, S., Leroux, Y. & Lagrost, C. One-Pot Electrografting of Mixed Monolayers with Controlled Composition. *J. Phys. Chem. C* **118**, 15919–15928 (2014).

[3] Malytskyi, V., Troian-Gautier, L., Mattiuzzi, A., Lambotte, S., Cornelio, B., Lagrost, C. & Jabin, I. Synthesis of a Calix[4]arene-Monodiazonium Salt for Surface Modification. *Eur. J. Org. Chem.* 6590–6595 (2018).

[4] Nikoobakht, B. & El-Sayed, M. A. Preparation and Growth Mechanism of Gold Nanorods (NRs) Using Seed-Mediated Growth Method. *Chem. Mater.* **15**, 1957–1962 (2003).

[5] He, J., Unser, S., Bruzas, I., Cary, R., Shi, Z., Mehra, R., Aron, K. & Sagle, L. The facile removal of ctab from the surface of gold nanorods. *Colloids Surf. B: Biointerfaces* **163**, 140–145 (2018).

[6] Hourahine, B., Aradi, B., Blum, V., Bonafé, F., Buccheri, A., Camacho, C., Cevallos, C., Deshaye, M. Y., Dumitrică, T., Dominguez, A., Ehlert, S., Elstner, M., van der Heide, T., Hermann, J., Irle, S., Kranz, J. J., Köhler, C., Kowalczyk, T., Kubař, T., Lee, I. S., Lutsker, V., Maurer, R. J., Min, S. K., Mitchell, I., Negre, C., Niehaus, T. A., Niklasson, A. M. N., Page, A. J., Pecchia, A., Penazzi, G., Persson, M. P., Řezáč, J., Sánchez, C. G., Sternberg, M., Stöhr, M., Stuckenberg, F., Tkatchenko, A., Yu, V. W.-z. & Frauenheim, T. DFTB+, a software package for efficient approximate density functional theory based atomistic simulations. *J. Chem. Phys.* **152**, 124101 (2020).

[7] Fihey, A., Hettich, C., Touzeau, J., Maurel, F., Perrier, A., Köhler, C., Aradi, B. & Frauenheim, T. Scc-dftb parameters for simulating hybrid gold-thiolates compounds. *J. Comput. Chem* **36**, 2075–2087 (2015).

[8] Vuong, V. Q., Madridejos, J. M. L., Aradi, B., Sumpter, B. G., Metha, G. F. & Irle, S. Density-functional tight-binding for phosphine-stabilized nanoscale gold clusters. *Chem. Sci.* **11**, 13113–13128 (2020).

[9] Monkhorst, H. J. & Pack, J. D. Special points for Brillouin-zone integrations. *Phys. Rev. B* **13**, 5188–5192 (1976).

[10] Ruud, K. & Thorvaldsen, A. J. Theoretical approaches to the calculation of Raman optical activity spectra. *Chirality* **21**, E54–E67 (2009).

[11] Smidstrup, S., Markussen, T., Vancraeyveld, P., Wellendorff, J., Schneider, J., Gunst, T., Verstichel, B., Stradi, D., Khomyakov, P. A., Vej-Hansen, U. G. *et al.* Quantumatk: An integrated platform of electronic and atomic-scale modelling tools. *J. Phys.: Condens. Matter* **32**, 015901 (2020).

[12] Ashcroft, N. & Mermin, N. *Solid state physics* (1976).

[13] Elstner, M., Porezag, D., Jungnickel, G., Elsner, J., Haugk, M., Frauenheim, T., Suhai, S. & Seifert, G. Self-consistent-charge density-functional tight-binding method for simulations of complex materials properties. *Phys. Rev. B* **58**, 7260 (1998).

[14] Niehaus, T. A., Elstner, M., Frauenheim, T. & Suhai, S. Application of an approximate density-functional method to sulfur containing compounds. *J. Mol. Struct.: THEOCHEM* **541**, 185–194 (2001).

[15] Kresse, G. & Furthmüller, J. Efficiency of ab-initio total energy calculations for metals and semiconductors using a plane-wave basis set. *Comput. Mater. Sci.* **6**, 15–50 (1996).

[16] Kresse, G. & Furthmüller, J. Efficient iterative schemes for ab initio total-energy calculations using a plane-wave basis set. *Phys. Rev. B* **54**, 11169–11186 (1996).

[17] Bruni, S., Bandini, A. L., Cariati, F. & Speroni, F. A revision on gold(i)-carbon stretching frequencies. *Inorganica Chim. Acta* **203**, 127–128 (1993).

[18] Shaw, C. F. & Tobias, R. S. Bonding in methylgold(i) and trimethylgold(iii) compounds. nuclear magnetic resonance, raman, and infrared spectra and normal coordinates1. *Inorg. Chem.* **12**, 965–978 (1973).